

## Flocking turbulence of microswimmers in confined domains

L. Puggioni <sup>1</sup>, G. Boffetta<sup>1,2</sup> and S. Musacchio <sup>1,\*</sup>

<sup>1</sup>*Dipartimento di Fisica and INFN, Università degli Studi di Torino, via P. Giuria 1, 10125 Torino, Italy*

<sup>2</sup>*Okinawa Institute of Science and Technology, 1919-1 Tancha, Onna-son, Okinawa 904-0495, Japan*

 (Received 21 December 2022; revised 31 March 2023; accepted 5 May 2023; published 23 May 2023)

We extensively study the Toner-Tu-Swift-Hohenberg model of motile active matter by means of direct numerical simulations in a two-dimensional confined domain. By exploring the space of parameters of the model we investigate the emergence of a new state of active turbulence which occurs when the aligning interactions and the self-propulsion of the swimmers are strong. This regime of *flocking turbulence* is characterized by a population of few strong vortices, each surrounded by an island of coherent flocking motion. The energy spectrum of flocking turbulence displays a power-law scaling with an exponent which depends weakly on the model parameters. By increasing the confinement we observe that the system, after a long transient characterized by power-law-distributed transition times, switches to the ordered state of a single *giant vortex*.

DOI: [10.1103/PhysRevE.107.055107](https://doi.org/10.1103/PhysRevE.107.055107)

### I. INTRODUCTION

The study of motile active matter as an example of nonequilibrium statistical system has become increasingly important in the last years [1,2]. A wide class of active systems, like bacterial suspensions [3,4], microtubule-kinesin mixtures [5,6], cell tissues [7], vibrated disks and rods [8,9], Janus particles [10], and motile colloids [11], exhibits a very rich phenomenology of collective motions. Many of them can develop a complex spatiotemporal chaos, called active turbulence for its resemblance to inertial turbulence in fluids [12]. To describe active turbulence a variety of continuum models has been proposed [13,14] that can be divided in polar models, characterized by a vectorial order parameter, and nematic models, with a rank-2 tensorial order parameter [15,16]. In general, this continuum approach allows the use of hydrodynamical tools to investigate active matter dynamics.

The nature of the order parameter in the models produces a peculiar phenomenology. In particular, polar systems can exhibit a long-range ordered phase, with the constituent particles aligning to each other and moving with constant speed, a phenomenon known as flocking [2]. Since the original works by Vicsek [17] and Toner and Tu [18,19], the investigation of flocking dynamics has attracted the attention of physicists, both from an experimental [11,20,21] and a theoretical [22–25] point of view. In recent years, the Toner-Tu (TT) model has been subject of various generalizations, to incompressible flows [26–28], to curved surfaces [29], to the high-Reynolds number limit [30,31], and to quenched disorder [32,33].

In particular, a modified version of the incompressible Toner-Tu model has been proposed to describe the dynamics of dense microswimmers suspensions [4,34,35]. In this version, denoted as Toner-Tu-Swift-Hohenberg (TTSH) model,

the Landau force and the self-advection term of the TT model are combined with the Swift-Hohenberg (SH) operator for pattern formation [36]. In two dimensions, the TTSH model exhibits a very rich phenomenology which encompasses different regimes: Stationary vortex lattice [37,38], isotropic mesoscale turbulence [39–42], and turbulent crystal-like regime [37,43].

Linear stability analysis [44] predicts that the regime of uniform flocking (which is present in the original Toner-Tu model) is destabilized by the Swift-Hohenberg operator, and therefore it cannot be observed in the TTSH model. Nonetheless, recent works [45–47] have shown that, if the aligning interactions between swimmers are sufficiently strong, the TTSH model displays the emergence of an inhomogeneous regime characterized by the presence of large-scale, isolated vortices, surrounded by regions of small vortices and elongated vortical structures, called *vorticity streaks*.

Another mechanism which is known to influence the self-organization process in active matter is the confinement by physical boundaries [48]. While numerical studies of the TTSH model are usually performed in the absence of boundaries, recent experiments with bacterial suspensions have shown that confinement can promote the formation of complex collective motion [21,49–51]. Moreover, a numerical study of the TTSH model showed that, when the flow is confined in circular bounded domains, the swimmers can self-organize in a state of global circular flocking characterized by a single, giant vortex [52].

In this paper, we present a detailed investigation of the inhomogeneous regime of large-scale vortices. We show that these structures arise from local attempts to organize the flow in configurations of circular flocking. The interactions between the flocking vortices give rise to a new dynamical regime that we call *flocking turbulence*. By means of an extensive exploration of the parameter space we highlight the importance of the interplay between the Landau force and the nonlinear advection term to induce the transition from

\*Corresponding author: [stefano.musacchio@unito.it](mailto:stefano.musacchio@unito.it)

the regime of isotropic mesoscale turbulence toward flocking turbulence.

The remainder of this paper is organized as follows. In Sec. II we introduce the model and the numerical method. In Sec. III we explore the parameters of the model and we report the conditions under which the transition to flocking turbulence is observed. In Sec. IV we study the effect of confinement and its role in the transition to the giant vortex regime. Finally, Sec. V is devoted to conclusions.

## II. TONER-TU-SWIFT-HOHENBERG MODEL

The Toner-Tu-Swift-Hohenberg (TTSH) model describes the effective dynamics of a dense suspension of elongated microswimmers as a polar active fluid, governed by an incompressible Navier-Stokes-like equation for the coarse-grained collective velocity field  $\mathbf{u}$ :

$$\partial_t \mathbf{u} + \lambda \mathbf{u} \cdot \nabla \mathbf{u} = -\nabla p - (\alpha + \beta |\mathbf{u}|^2 + \Gamma_2 \nabla^2 + \Gamma_4 \nabla^4) \mathbf{u}. \quad (1)$$

The pressure term  $\nabla p$  ensures the incompressibility of the flow,  $\nabla \cdot \mathbf{u} = 0$ , since in dense suspensions one can neglect density fluctuations. The Toner-Tu terms are the Landau force  $-(\alpha + \beta |\mathbf{u}|^2) \mathbf{u}$  and the self-advection term  $\lambda \mathbf{u} \cdot \nabla \mathbf{u}$ , while the Swift-Hohenberg operator is  $-(\Gamma_2 \nabla^2 + \Gamma_4 \nabla^4)$ . The coefficients  $\lambda, \alpha, \beta, \Gamma_2, \Gamma_4$  are phenomenological parameters related to the properties of the microswimmers, the surrounding fluid and their interaction [53,54]. The self-advection parameter  $\lambda$  is related both to the motility of the swimmers [54], with  $\lambda > 1$  ( $\lambda < 1$ ) corresponding to pushers (pullers), respectively [12], and to aligning interactions between the swimmers. Strong interactions lead to large positive values of  $\lambda$ , large negative values of  $\alpha$  and reduce the value of  $\Gamma_2$ .

In the absence of boundaries, for  $\alpha < 0$  the Landau force allows for two stationary, uniform solutions of Eq. (1). The first is the solution with null velocity, which is linearly unstable for  $\alpha < 0$  [35]. The second is the state of uniform flocking  $\mathbf{u}(\mathbf{x}, t) = U \hat{\mathbf{e}}_u$  with constant velocity  $U = \sqrt{-\alpha/\beta}$  oriented in an arbitrary direction  $\hat{\mathbf{e}}_u$ . The stability of this state depends on the sign of the parameters  $\Gamma_2$  and  $\Gamma_4$  of the Swift-Hohenberg operator. For  $\Gamma_2 < 0$  and  $\Gamma_4 > 0$ , the solution with constant uniform velocity is linearly stable. On the contrary, for  $\Gamma_2, \Gamma_4 > 0$  the Swift-Hohenberg operator destabilizes the ordered state and it generates structures with characteristic scale  $\Lambda = 2\pi\sqrt{2\Gamma_4/\Gamma_2}$  [35,36,44].

The linear stability analysis of the state with uniform velocity  $U$  predicts that the most unstable mode has the form of alternated jets of width  $\Lambda/2$ , perpendicular to the direction of the mean flow  $\hat{\mathbf{e}}_u = 0$ . In the case of initial null velocity, the most unstable mode is a square lattice of alternated vortices, with wavelength  $\Lambda$  [35].

The scale  $\Lambda$  corresponds to the typical size of the mesoscale vortices observed in experiments [4,34]. Rescaling (1) with the characteristic scale  $\Lambda$  and velocity  $U$ , the three independent dimensionless parameters of the model are  $\lambda, \alpha\Lambda/U$  and  $\Gamma_2/\Lambda U$ . Note that since the TTSH has a characteristic velocity  $U$  it is not Galilean invariant. Therefore (1) is allowed to have  $\lambda \neq 1$ , at variance with the Navier-Stokes equation.

TABLE I. Parameters of the simulations. In the set of simulations  $AxRy$  we vary  $\alpha$  and  $R$  and we keep fixed  $\lambda$ . In the set of simulations  $LxRy$  we vary  $\lambda$  and we keep fixed  $\alpha$  and  $R$ . The simulations  $AxP$  are performed with periodic boundary conditions, i.e., without the circular confinement.

| Run  | $\alpha$ | $\lambda$ | $R/\Lambda$ | $N$  | Run   | $\alpha$ | $\lambda$ | $R/\Lambda$ | $N$  |
|------|----------|-----------|-------------|------|-------|----------|-----------|-------------|------|
| A1R1 | -0.25    | 3.5       | 16          | 512  | A7R1  | -1.75    | 3.5       | 16          | 512  |
| A1R2 | -0.25    | 3.5       | 23          | 1024 | A7R2  | -1.75    | 3.5       | 23          | 1024 |
| A1R3 | -0.25    | 3.5       | 31          | 1024 | A7R3  | -1.75    | 3.5       | 31          | 1024 |
| A1R4 | -0.25    | 3.5       | 63          | 2048 | A7R4  | -1.75    | 3.5       | 63          | 2048 |
| A2R1 | -0.50    | 3.5       | 16          | 512  | A8R1  | -2.00    | 3.5       | 16          | 512  |
| A2R3 | -0.50    | 3.5       | 31          | 1024 | A8R2  | -2.00    | 3.5       | 23          | 1024 |
| A2R4 | -0.50    | 3.5       | 63          | 2048 | A8R3  | -2.00    | 3.5       | 31          | 1024 |
| A3R1 | -0.75    | 3.5       | 16          | 512  | A8R4  | -2.00    | 3.5       | 63          | 2048 |
| A3R3 | -0.75    | 3.5       | 31          | 1024 | L1R4  | -1.00    | 2.0       | 63          | 2048 |
| A3R4 | -0.75    | 3.5       | 63          | 2048 | L2R4  | -1.00    | 2.5       | 63          | 2048 |
| A4R1 | -1.00    | 3.5       | 16          | 512  | L3R4  | -1.00    | 3.0       | 63          | 2048 |
| A4R2 | -1.00    | 3.5       | 23          | 1024 | L4R4  | -1.00    | 3.5       | 63          | 2048 |
| A4R3 | -1.00    | 3.5       | 31          | 1024 | L5R4  | -1.00    | 4.0       | 63          | 2048 |
| A4R4 | -1.00    | 3.5       | 63          | 2048 | L6R4  | -1.00    | 4.5       | 63          | 2048 |
| A5R1 | -1.25    | 3.5       | 16          | 512  | L7R4  | -1.00    | 5.0       | 63          | 2048 |
| A5R2 | -1.25    | 3.5       | 23          | 1024 | L8R4  | -1.00    | 5.5       | 63          | 2048 |
| A5R3 | -1.25    | 3.5       | 31          | 1024 | L9R4  | -1.00    | 6.0       | 63          | 2048 |
| A5R4 | -1.25    | 3.5       | 63          | 2048 | L10R4 | -1.00    | 6.5       | 63          | 2048 |
| A6R1 | -1.50    | 3.5       | 16          | 512  | L11R4 | -1.00    | 7.0       | 63          | 2048 |
| A6R2 | -1.50    | 3.5       | 23          | 1024 | A1P   | -0.25    | 3.5       | —           | 2048 |
| A6R3 | -1.50    | 3.5       | 31          | 1024 | A4P   | -1.00    | 3.5       | —           | 2048 |
| A6R4 | -1.50    | 3.5       | 63          | 2048 | A7P   | -1.75    | 3.5       | —           | 2048 |

To facilitate the comparison between the TTSH model and the experiments, in the numerical simulations it is customary to keep fixed the parameters  $\Gamma_2$  and  $\Gamma_4$ , which determine the scale  $\Lambda$ . Varying the parameter  $\alpha$  at fixed  $\beta$  allows to match the velocity scale  $U$  with the typical velocity of the experiments. In the light of the interpretation of the parameters in terms of the properties of the microswimmers [53,54] an increase of the negative magnitude of  $\alpha$  and  $\lambda$  at fixed  $\Gamma_2$  corresponds to an increase of the aligning interactions.

### Numerical methods

The model (1) is numerically integrated in two dimensions by a standard pseudospectral method in the vorticity-velocity formulation with a 1/2 dealiasing for the cubic nonlinearity, and a fourth-order Runge-Kutta time stepping. Confinement in a circular domain is imposed by the penalization method [55,56], which consists in modeling the region outside the domain as a porous medium with vanishing permeability. This is equivalent to imposing a no-slip boundary condition at the border of the circular domain. To this aim, the term  $-\frac{1}{\tau} \mathcal{M}(\mathbf{x}) \mathbf{u}$  is added to Eq. (1), where  $\tau$  is the permeability time and the mask field  $\mathcal{M}(\mathbf{x})$  is equal to 0 and 1, respectively, inside and outside a circular domain of radius  $R$  [57].

We performed two main sets of simulations. In the first, indicated with  $AxRy$  (see Table I) we fix  $\lambda = 3.5$  and vary

both  $\alpha$  in the range from  $\alpha = -0.25$  to  $\alpha = -2$  and  $R$  in the range from  $R = 16\Lambda$  to  $R = 63\Lambda$ . In the second set, named  $Lx$ , we fix both  $\alpha = -1.00$  and  $R = 63\Lambda$ , and vary  $\lambda$  in the range from  $\lambda = 2$  to  $\lambda = 7$ , as shown in Table I. An additional set of 269 simulations was performed for the case  $A6R1$  to study the transition time to the circular flocking state. We also performed three simulations  $AxP$  with periodic boundary conditions (i.e., without confinement) and null mean velocity as a reference case to study the effects of the confinement. The domains with radius  $R = 63\Lambda$ ,  $R = \{31, 23\}\Lambda$ , and  $R = 16\Lambda$  are embedded in squared periodic domains of size  $L = \{160, 80, 40\}\Lambda$  with numerical resolutions  $N = \{2048, 1024, 512\}$ , respectively. The values of the other parameters are fixed as follows:  $\beta = 0.01$ ,  $\Gamma_2 = 2$ ,  $\Gamma_4 = 1$ . The characteristic scale is  $\Lambda = 2\pi$ . The permeability time of the penalization term is  $\tau = 0.001$ , which is smaller than any dynamical time. In all the simulations, the initial condition is a null velocity field with a small amplitude random perturbation superimposed.

We identify vortices by means of the standard Okubo-Weiss parameter [58,59]  $Q = (\partial_{xy}^2\psi)^2 - (\partial_x^2\psi)(\partial_y^2\psi)$ , where  $\psi$  is the stream function [i.e.,  $\mathbf{u} = (\partial_y\psi, -\partial_x\psi)$ ] and  $\omega = -\nabla^2\psi$  is the vorticity.  $Q < 0$  corresponds to vortical regions, while  $Q > 0$  to regions dominated by shear. Vortices are defined as connected regions of the space where  $Q \leq -Q^*$  and the threshold value  $Q^*$  is chosen as three times the root-mean-squared (rms) value of the  $Q$  field. We checked that our results do not depend on the precise value of  $Q^*$ . The Okubo-Weiss criterion has been already used in TTSH simulations for the study of its Lagrangian properties [46,60].

### III. TRANSITION TOWARD FLOCKING TURBULENCE

The early stage of the evolution of the system is driven by the linear term  $\mathcal{L}\mathbf{u} = -\alpha\mathbf{u} - \Gamma_2\nabla^2\mathbf{u} - \Gamma_4\nabla^4\mathbf{u}$  and it is characterized by an exponential growth of the rms values of the velocity and vorticity. Since the simulations are initialized with a small random perturbation of the null velocity field, in this stage we observe the formation of a regular square lattice of vortices with alternating signs, in agreement with the predictions of the linear stability analysis [35]. This phase ends when the nonlinear terms become relevant. The cubic damping term of the Landau force arrests the exponential growth of the velocity and the self-advection term causes the chaotic motion of the vortices [37,38]. This regime is characterized by an homogeneous, disordered population of small vortices [see Figs. 1(a) and 1(b)], which move randomly, hence it is called mesoscale turbulence [4]. The vortices are uniformly distributed in the circular domain, with a high vortex number density  $n$  (defined as the number of vortices per unit area).

For moderate negative values of  $\alpha$  ( $-1 \lesssim \alpha < 0$ ) the regime of mesoscale turbulence is observed to persist for arbitrarily long simulation times. This is confirmed by the temporal evolution of the rms velocity  $u_{\text{rms}}$ , the rms vorticity  $\omega_{\text{rms}}$ , and the vortex density  $n$ , which remain statistically stationary after the initial transient, as shown in Fig. 2 for the case  $A1R4$ .

While it is not possible to establish a precise threshold value of  $\alpha$  for the persistence of the state of mesoscale turbulence, we observe that the behavior of the system changes

qualitatively at increasing the negative amplitude of  $\alpha$ . As shown in Figs. 2(b) and 2(c) for the cases  $A4R4$  and  $A7R4$ , for  $\alpha \lesssim -1$  both the rms vorticity and the number of vortices, after a peak at  $t \simeq 20\Lambda/U$ , decrease with time but their ratio (i.e., the average vorticity of the vortices) remains approximately constant. The rms velocity grows slowly in time [see Fig. 2(a)] and it achieves a stationary value at long times ( $t > 50\Lambda/U$ ).

For large negative amplitude of  $\alpha$  (e.g., for  $\alpha = -1.75$ ), the system achieves a strongly inhomogeneous state [61], characterized by few isolated vortices which move in the domain and elongate filaments called vorticity streaks [45] [see Fig. 1(e)]. Each vortex is surrounded by a wide region of coherent circular motion with constant speed  $U = \sqrt{-\alpha/\beta}$ . The vorticity streaks are observed in the peripheral regions of these vortices, and they are preferentially aligned in the transverse direction with respect to the circular motion. The flow is organized in large-scale structures, which are evident in the stream function shown in Fig. 1(f). Local dense vortex clusters are still present between these structures and close to the boundary of the domain.

The formation of this state can be interpreted as the emergence of different local attempts by the system to self-organize the flow in states of circular flocking. This process occurs independently in different regions of the domain, producing large vortices with either positive or negative sign. The Swift-Hohenberg operator is too weak to suppress completely the flocking tendency of the system, but it is still able to destabilize the peripheral regions of the vortices. Indeed, linear stability analysis of a global polar state predicts the appearance of a transverse pattern with respect to the mean flow with wavelength  $\Lambda$  [35]. The streaks observed in Fig. 1(e) correspond to this pattern, distorted by the advection produced by the other vortices. Since this regime is characterized by the chaotic interaction between the flocking vortices, we call it *flocking turbulence*.

The nonlinear self-advection term  $\lambda\mathbf{u} \cdot \nabla\mathbf{u}$  plays a crucial role in the development of flocking turbulence. To address this issue, we performed a second set of simulations keeping fixed  $\alpha = -1$  and varying  $\lambda$  in the range from 2 to 7. The temporal evolution of the rms velocity, vorticity and vortex density is shown in Fig. 3 for three different values of  $\lambda$  (simulations  $L1R4$ ,  $L4R4$ ,  $L7R4$ ). The rms velocity is almost unaffected by the change of  $\lambda$ . After an initial growth, it reaches approximately similar asymptotic values [for the case  $L7R4$  the stationary regime is achieved at time longer than the time shown in Fig. 3(a)]. The rms vorticity and vortex density, shown in Figs. 3(b) and 3(c), display a decrease after the initial peak at  $t \simeq 12\Lambda/U$ . At time  $t > 50\Lambda/U$  they reach different asymptotic values which decrease at increasing  $\lambda$ . This is qualitatively similar to what observed at increasing the intensity of  $|\alpha|$  [cf. Figs. 2(b) and 2(c)].

The dependence of the asymptotic values of rms velocity, vorticity, and vortex density as a function of the parameter  $\alpha$  and  $\lambda$  is shown in Figs. 4 and 5, respectively. The asymptotic values are computed as time average of the instantaneous values in the stationary regime and the error-bars are defined as the largest deviation from the mean value observed in the same time interval. The transition between the two regimes of mesoscale and flocking turbulence is evident in

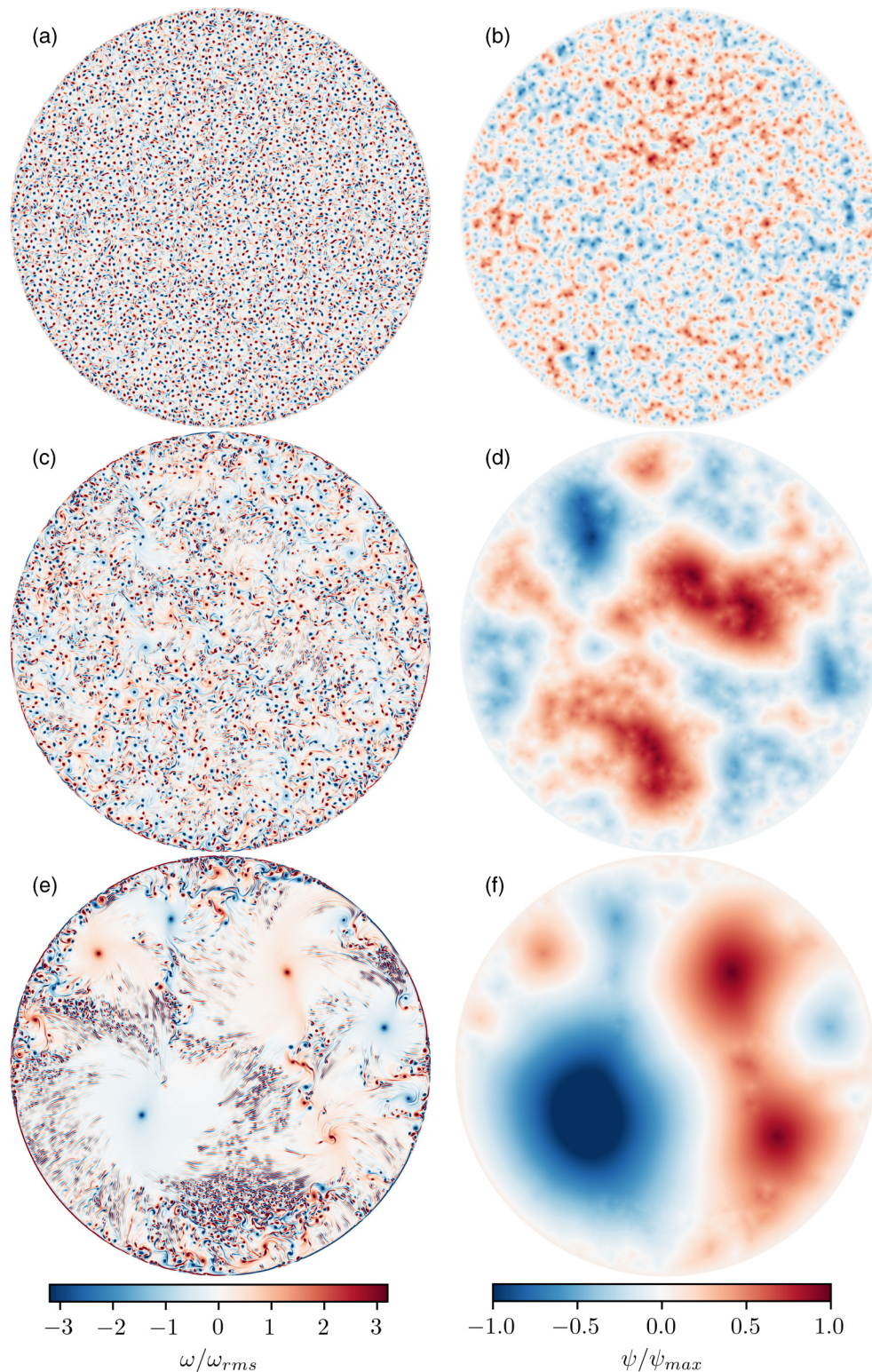


FIG. 1. Vorticity fields  $\omega$  (left) and stream function  $\psi$  (right), in the stationary regimes of the simulations with (a, b)  $\alpha = -0.25$  (AIR4), (c, d)  $\alpha = -1.00$  (A4R4), and (e, f)  $\alpha = -1.75$  (A7R4). Here  $\lambda = 3.5$  and  $R = 63\Lambda$ .

the dependence of the  $u_{\text{rms}}$  on  $\alpha$ . In the regime of flocking turbulence, at large negative values of  $\alpha$  the ratio between  $u_{\text{rms}}$  and  $U = \sqrt{-\alpha/\beta}$  is almost constant, meaning that  $u_{\text{rms}}$  grows proportionally to  $\sqrt{|\alpha|}$ . Conversely, at small values of  $|\alpha|$  the ratio  $u_{\text{rms}}/U$  increases, in agreement with the results of

previous studies of the mesoscale turbulence regime [41]. We find that  $u_{\text{rms}}$  is almost independent of  $\lambda$ .

Both the rms vorticity and the vortex density decrease by increasing the magnitude of  $|\alpha|$ , in agreement with the qualitative observation that the number of vortices decreases

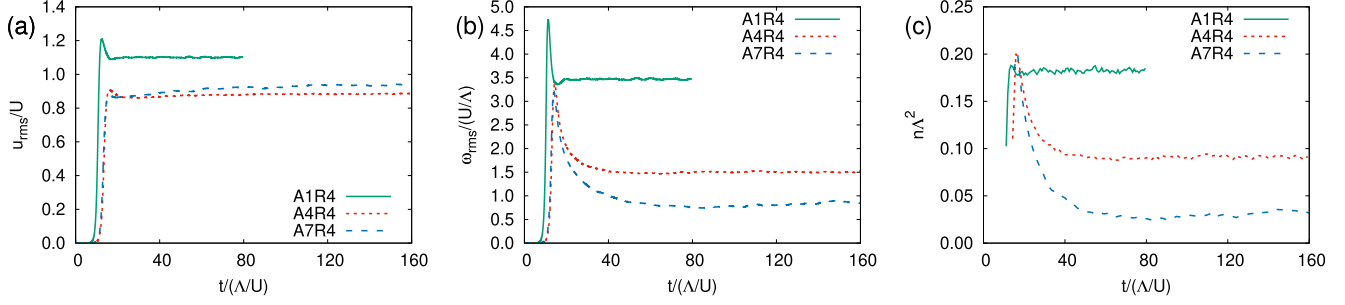


FIG. 2. Time evolution of (a) the rms velocity  $u_{\text{rms}}$ , (b) rms vorticity  $\omega_{\text{rms}}$ , and (c) vortex density  $n$  in the numerical simulations with  $\alpha = -0.25$  (A1R4, green solid line),  $\alpha = -1.00$  (A4R4, red dotted line), and  $\alpha = -1.75$  (A7R4, blue dashed line). Here  $\lambda = 3.5$  and  $R = 63\Lambda$ .

as shown in Fig. 1. A similar behavior is observed also by increasing the strength of the self-advection: Larger values of  $\lambda$  correspond to lower  $\omega_{\text{rms}}$  and  $n$ . The above results suggest that the transition from mesoscale turbulence to flocking turbulence is not solely due to the increase of the strength of the Landau force  $\alpha$ , but it requires also a strong enough self-advection (i.e., nonlinearity).

Further insights on this transition are given by the distribution of kinetic energy among different spatial scales, which is quantified by the energy spectrum

$$E(k) = \frac{1}{2} \sum_{|\mathbf{q}| \in [k, k + \Delta k]} |\mathcal{F}(\mathbf{u})(\mathbf{q})|^2, \quad (2)$$

where  $\mathcal{F}(\mathbf{u})$  indicates the Fourier transform velocity field and the sum is performed over all the modes  $\mathbf{q}$  in the shell  $|\mathbf{q}| \in [k, k + \Delta k]$  and  $\Delta k = 2\pi/L$ .

In the mesoscale turbulence regime,  $E(k)$  peaks around the characteristic wave number  $k_{\text{max}} \simeq 2\pi/\Lambda$  (see Fig. 6). Increasing the magnitude of  $|\alpha|$  the peak  $k_{\text{max}}$  of the spectrum shifts toward smaller wave numbers  $k_{\text{max}} < 2\pi/\Lambda$ , in agreement with previous findings [39–41].

In the regime of flocking turbulence (for  $|\alpha| \gtrsim 1$ ), we observe a qualitative change in the spectrum. The energy spectrum develops a power-law behavior  $E(k) \sim k^{-\delta}$  at intermediate wave numbers  $k_{\text{max}} \ll k \ll 2\pi/\Lambda$ , with a spectral exponent  $\delta$  which is close to the theoretical value  $\delta = 3/2$  predicted and observed in Ref. [47]. At large, negative values of  $\alpha$  we observe a slight increase of  $\delta$ , which exceeds the value  $3/2$ . At the same time, the wave number  $k_{\text{max}}$  becomes almost constant and it is close to the wave number  $2\pi/R$ . As we

will discuss in the next section, these effects are due to the confinement.

Interestingly, we find that the decrease of peak of the energy spectrum  $k_{\text{max}}$  and the development of the intermediate power-law behavior is observed also at increasing the parameter  $\lambda$  at fixed  $\alpha$ . This is a further clue that the transition from mesoscale to flocking turbulence is determined by the interplay between the Landau force and the self-advection term.

The role of these terms in the transition is highlighted by the analysis of the spectral contributions to the evolution of the energy spectrum

$$\partial_t E(k) = T_\lambda(k) + T_L(k) + T_{\text{SH}}(k) + T_M(k), \quad (3)$$

where

$$T_\lambda(k) = - \sum \Re[\mathcal{F}(\mathbf{u})^* \mathcal{F}(\lambda \mathbf{u} \cdot \nabla \mathbf{u})], \quad (4)$$

$$T_L(k) = - \sum \Re[\mathcal{F}(\mathbf{u})^* \mathcal{F}(\alpha \mathbf{u} + \beta |\mathbf{u}|^2 \mathbf{u})], \quad (5)$$

$$T_{\text{SH}}(k) = - \sum \Re[\mathcal{F}(\mathbf{u})^* \mathcal{F}(\Gamma_2 \nabla^2 \mathbf{u} + \Gamma_4 \nabla^4 \mathbf{u})], \quad (6)$$

$$T_M(k) = - \sum \Re \left[ \mathcal{F}(\mathbf{u})^* \mathcal{F} \left( \frac{1}{\tau} \mathcal{M} \mathbf{u} \right) \right], \quad (7)$$

correspond, respectively, to self-advection, Landau, Swift-Hohenberg and penalization terms,  $\Re$  represents the real part and the sum is performed over all the wave numbers  $\mathbf{q}$  in the shell  $|\mathbf{q}| \in [k, k + \Delta k]$  and  $\Delta k = 2\pi/L$ .

In the regime of mesoscale turbulence,  $T_{\text{SH}}$  injects energy at wave numbers  $k \simeq \pi/\Lambda$ , the self-advection term  $T_\lambda$  redistributes the energy to smaller wave numbers ( $k \simeq 0.4\pi/\Lambda$ ) and the Landau term  $T_L$  subtracts energy at all scales (Fig. 7).

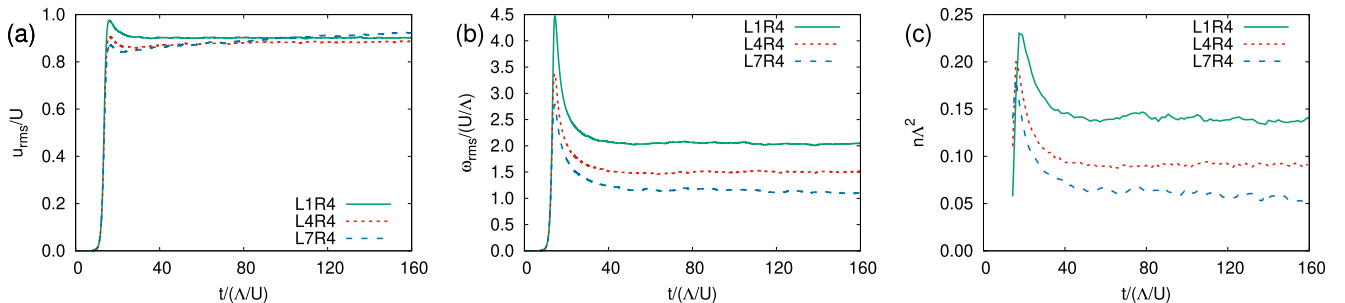


FIG. 3. Time evolution of (a) the rms velocity  $u_{\text{rms}}$ , (b) rms vorticity  $\omega_{\text{rms}}$  and (c) vortex density  $n$  in the numerical simulations with  $\lambda = 2.0$  (L1R4, green solid line),  $\lambda = 3.5$  (L4R4, red dotted line) and  $\lambda = 5.0$  (L7R4, blue dashed line). Here  $\alpha = -1.00$  and  $R = 63\Lambda$ .

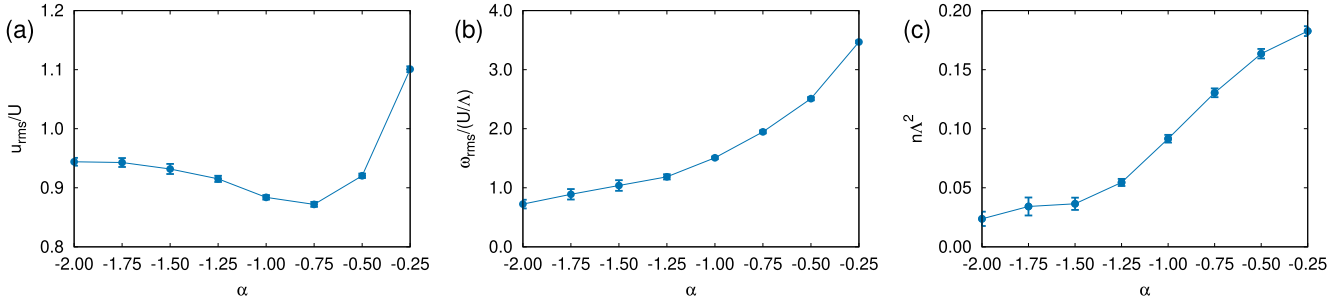


FIG. 4. Asymptotic values of (a) rms velocity  $u_{rms}$ , (b) rms vorticity  $\omega_{rms}$ , and (c) vortex density  $n$  as a function of  $\alpha$  in the numerical simulation  $AxR4$  with  $\lambda = 3.5$  and  $R = 63\Lambda$ .

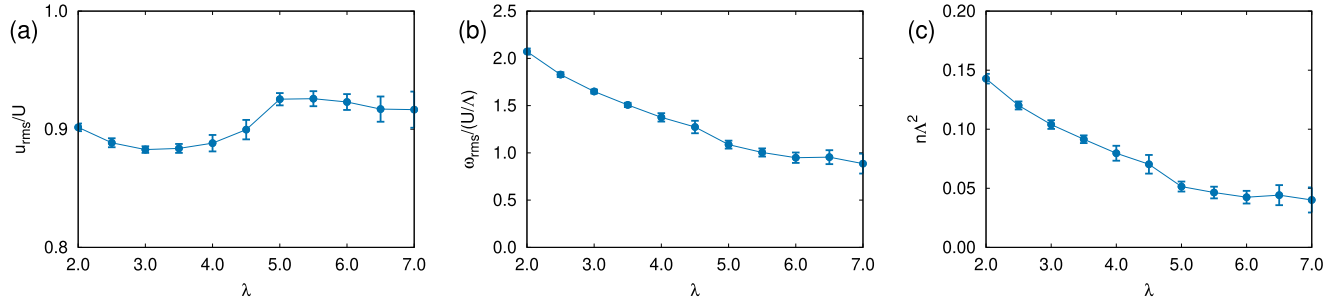


FIG. 5. Asymptotic values of (a) rms velocity  $u_{rms}$ , (b) rms vorticity  $\omega_{rms}$ , and (c) vortex density  $n$  as a function of  $\lambda$  in the numerical simulations  $LxR4$  with  $\alpha = -1.00$  and  $R = 63\Lambda$ .

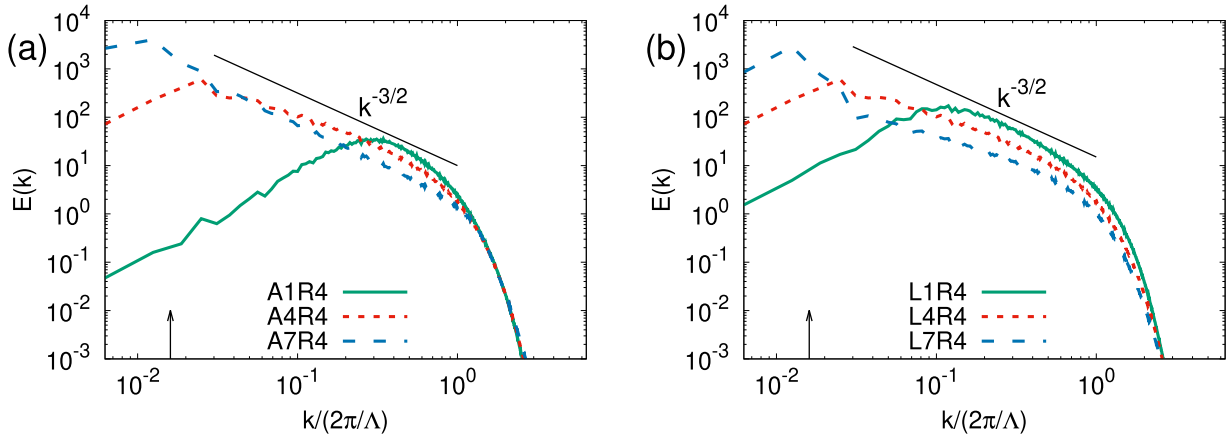


FIG. 6. Kinetic energy spectra, averaged in the stationary regimes of the simulations with (a) fixed  $\lambda = 3.5$  and (b) fixed  $\alpha = -1.00$ . Here  $R = 63\Lambda$ . The arrow indicates the wave number  $2\pi/R$ .

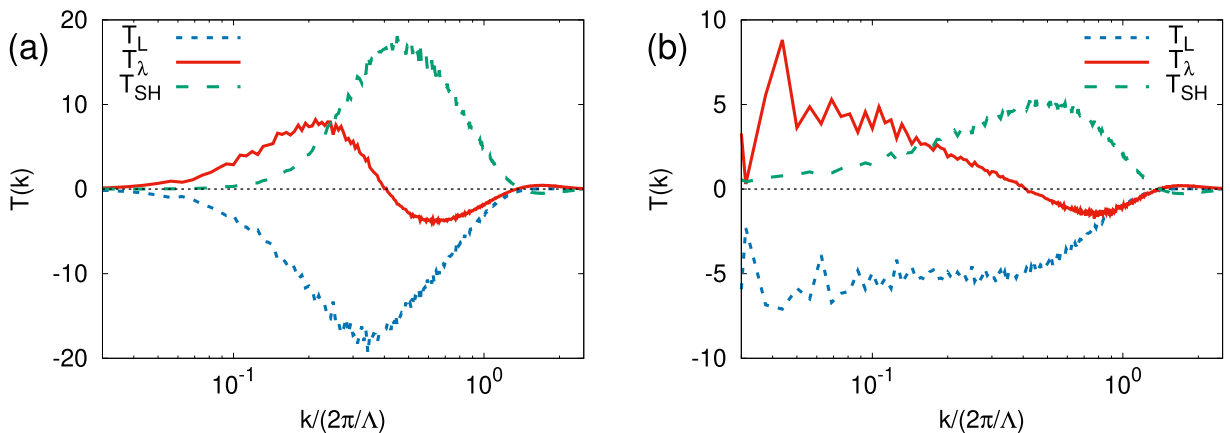


FIG. 7. Spectral terms  $T_\lambda$ ,  $T_L$ , and  $T_{SH}$  in the stationary regimes of the simulations in the regime of mesoscale turbulence (a) with  $\alpha = -0.25$ ,  $\lambda = 3.5$  (A1R4) and in the regime of flocking turbulence (b) with  $\alpha = -1.00$ ,  $\lambda = 5$  (L7R4). Here  $R = 63\Lambda$ .

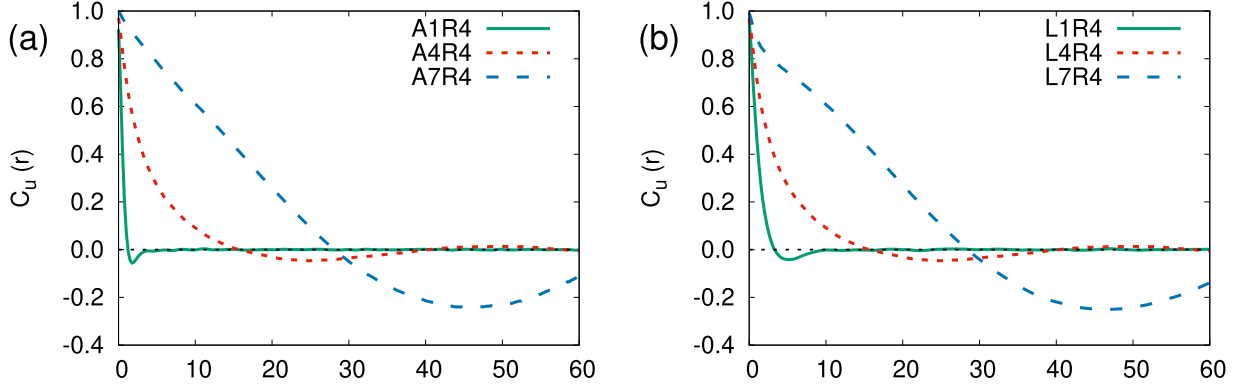


FIG. 8. Correlations functions of the velocity field  $C_u(r)$  in the stationary regimes of the simulations with (a) fixed  $\lambda = 3.5$  and (b) fixed  $\alpha = -1.00$ . Here  $R = 63\Lambda$ .

This is in agreement with previous findings [39]. The effects of these terms are similar in the regime of flocking turbulence, but  $T_L$  and  $T_\lambda$  are active on a broader range of wave numbers. In particular,  $T_\lambda$  transfers the kinetic energy injected at small scales by the  $T_{SH}$  term to large-scale. In both the regimes, the penalization term  $T_M(k)$  (not shown) is negligible at all wave numbers.

The growth of the integral scale of the flow, signaled by the reduction of  $k_{max}$ , can be quantified by the analysis of the correlation functions of the velocity field

$$C_u(r) = \frac{\langle \mathbf{u}(\mathbf{x}) \cdot \mathbf{u}(\mathbf{x}') \rangle}{\langle |\mathbf{u}(\mathbf{x})|^2 \rangle}, \quad (8)$$

with  $r = \|\mathbf{x} - \mathbf{x}'\|$ , and angular brackets indicating average over space and time (in the stationary regime). We remark that correlation functions are a well established tool for the study of flocking phenomena [62].

The velocity correlation function, plotted in Fig. 8, displays a negative minimum which allows to define a velocity correlation scale  $\xi$  given by the first zero crossing of  $C_u$ . The dependence of  $\xi$  on the parameters  $\alpha$  and  $\lambda$  is reported in Fig. 9. Both reducing  $\alpha$  at fixed  $\lambda$  and increasing  $\lambda$  at fixed  $\alpha$  we observe a sharp increase of  $\xi$  from values comparable to  $\Lambda$  to values of the order  $30\Lambda$ , which indicates the transition from the mesoscale regime to the flocking turbulence. At large

values of  $\Lambda$  and large negative values of  $\alpha$  we also observe a saturation of the correlation scale to an asymptotic value  $\xi \approx 30\Lambda$  which is comparable with the radius of the circular domain ( $R = 63\Lambda$ ).

#### IV. ROLE OF CONFINEMENT AND CIRCULAR FLOCKING

The saturation of the correlation length and of the peak of the energy spectrum  $k_{max}$  suggests that the geometrical confinement of the bacterial turbulence influences significantly its dynamics. In this section we pursue the investigation of the effects of the confinement presenting the results of simulations of the TTSH model in circular domains at varying the radius  $R$  of the domain.

In Fig. 10 we compare the asymptotic stationary values of the rms velocity  $u_{rms}$ , rms vorticity  $\omega_{rms}$  and vortex density  $n$  as a function of the domain size  $R$  for three sets of simulations in the regime of mesoscale turbulence ( $\alpha = -0.25$ ), in the transition regime ( $\alpha = -1.00$ ) and in the regime of flocking turbulence ( $\alpha = -1.75$ ). The parameter  $\lambda = 3.5$  is fixed for all the simulations. The asymptotic values presented in Fig. 9 are normalized with the corresponding values  $u_{rms0}$ ,  $\omega_{rms0}$ , and  $n_0$  obtained in the set of simulations  $AxP$  with identical parameters, performed in a large square domain with size

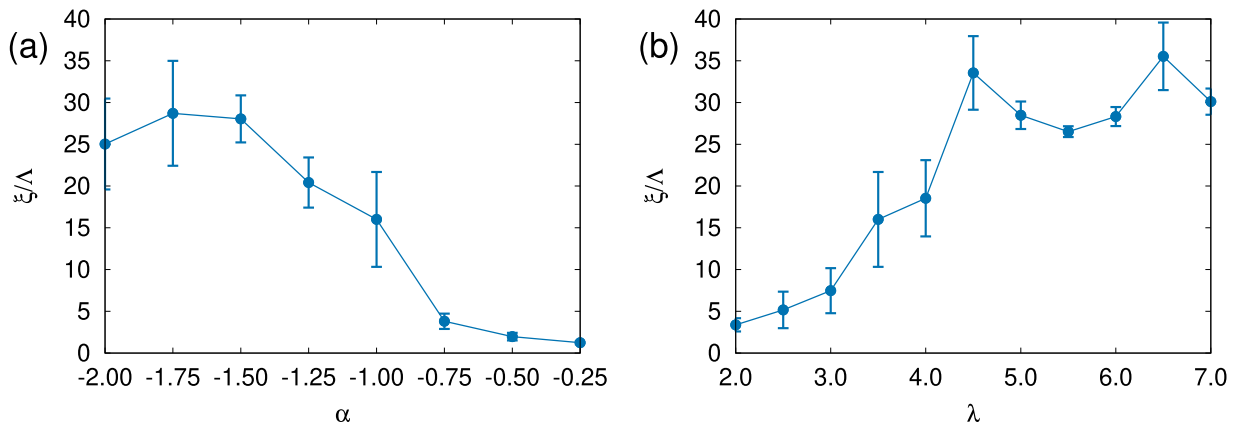


FIG. 9. Velocity correlation length  $\xi$ , in the stationary regimes of the simulations with (a) fixed  $\lambda = 3.5$  ( $AxR4$ ) and (b) fixed  $\alpha = -1.00$  ( $LxR4$ ). Here  $R = 63\Lambda$ .

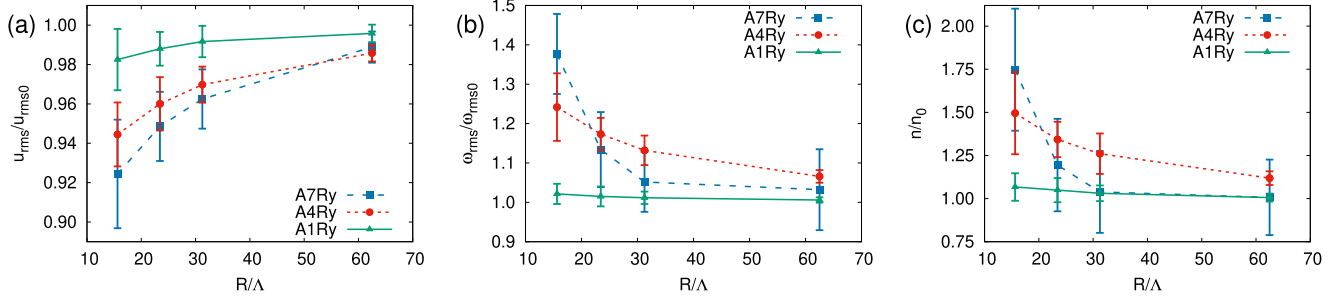


FIG. 10. Asymptotic values of (a) the rms velocity  $u_{rms}$ , (b) rms vorticity  $\omega_{rms}$ , and (c) vortex density  $n$  as a function of the confinement radius  $R$ . Here  $\lambda = 3.5$ .

$L = 160\Lambda$  and periodic boundary conditions, which is the typical setup for the numerical studies of the TTSH model.

The effects of the confinement are qualitatively similar for all the regimes: Increasing the confinement, i.e., reducing  $R$ , we observe a decrease of the asymptotic values of  $u_{rms}$  and an increase of  $\omega_{rms}$  and  $n$ . This effects can be ascribed to the interactions of the flow with the no-slip boundary. The friction with the boundary dissipates part of the energy, thus reducing  $u_{rms}$ . Close to the boundaries, the energy dissipation is accompanied by the production of small vortices, which causes an increase of  $\omega_{rms}$  and of the total number of vortices per unit area. These effects are stronger for the cases with smaller radius  $R$ , because of the larger ratio between the perimeter and the area of the domain.

Nonetheless, we observe significant quantitative differences. In the case of mesoscale turbulence ( $\alpha = -0.25$ ) the values of  $u_{rms}$ ,  $\omega_{rms}$ , and  $n$  vary weakly with  $R$  and they remain close to those of the simulations with periodic boundaries. Conversely, the values obtained in the flocking turbulence regime display a strong dependence on  $R$ . The weak influence of the confinement on the mesoscale turbulence can be explained by the observation that in this regime the correlation length  $\xi$  of the velocity field is approximately one order of magnitude smaller than  $R$ . Therefore the effects of the confinement are restricted to a small region close to the boundary. In the intermediate case ( $\alpha = -1$ ) the correlation length  $\xi$  is larger than in the mesoscale turbulence (see Fig. 9) and the effects of the confinement are stronger. In the flocking turbulence regime ( $\alpha = -1.75$ ) the values of  $u_{rms}$ ,  $\omega_{rms}$ , and  $n$  change rapidly when the radius  $R$  becomes smaller than the correlation length  $\xi \approx 30\Lambda$ .

The effect of the confinement is evident also in the energy spectra. In Fig. 11 we compare the spectral exponent  $\delta$  of the energy spectrum measured in simulations with different  $R$  and  $\alpha$ . In the set of simulations with  $\alpha = -1.25$  the exponent is almost independent of  $R$  and its value is close to the theoretical prediction  $3/2$  [47]. The independence of the spectra on  $R$  is observed also for  $\alpha > -1.25$  (not shown), which confirms that the effects of the confinement on the regime of mesoscale turbulence are weak.

In the regime of flocking turbulence the spectral exponent  $\delta$  varies significantly with  $R$  and  $\alpha$ . Decreasing the radius  $R$  we find that  $\delta$  grows up to an asymptotic value which increases with  $|\alpha|$ . We argue that the steepening of the energy spectrum due to the confinement can be related to the process of spectral energy condensation, i.e., of the accumulation of energy in

the lowest mode accessible to the system, whose wavelength is comparable to the size of the domain. This explains the discrepancy between the exponent of the energy spectra observed in our simulations and the results reported in Ref. [47]. The trend of the values of  $\delta$  at increasing  $R$  suggests the conjecture that the exponent attains an universal value  $\delta = 3/2$  in the limit of unconfined, infinite domain.

Recent studies [52] showed that in the case of strong confinement (i.e., small  $R$ ) the regime of flocking turbulence becomes metastable. After a long transient, it displays a sudden transition toward an ordered state of circular flocking, which corresponds to a single giant vortex which spans the whole domain [61]. The giant vortex is surrounded by an ordered pattern of vorticity streaks, aligned in the radial direction.

A convenient indicator of the transition to the giant vortex regime is provided by the vortex order parameter [21,63]

$$\Phi = \frac{\langle u_\varphi \rangle / \langle |\mathbf{u}| \rangle - 2/\pi}{1 - 2/\pi}, \quad (9)$$

which is defined in terms of the radial and angular components of the velocity field  $\mathbf{u} = u_r \hat{\mathbf{r}} + u_\varphi \hat{\boldsymbol{\phi}}$ . In the case of randomly oriented velocity field one has  $\Phi = 0$ , while  $\Phi = 1$  for a velocity field fully oriented in the angular direction.

In Fig. 12 we show the time evolution of  $\Phi$  of an ensemble of simulations with  $\alpha = -1.50$ ,  $\lambda = 3.5$ , and  $R = 16\Lambda$ ,

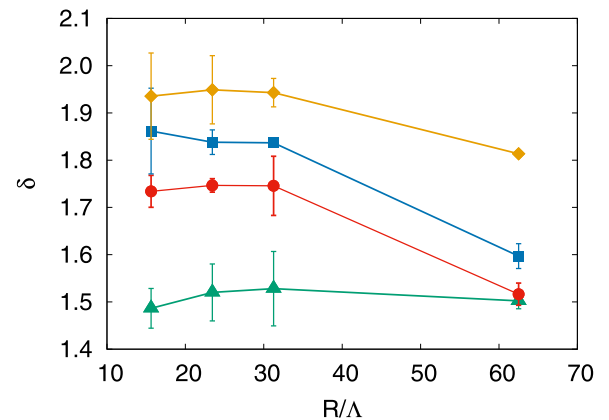


FIG. 11. Spectral exponent  $\delta$  as a function of confinement radius  $R$ , in the simulations with  $\lambda = 3.5$  and  $\alpha = -2.00$  (A8Ry, orange diamonds),  $\alpha = -1.75$  (A7Ry, blue squares),  $\alpha = -1.50$  (A6Ry, red circles), and  $\alpha = -1.25$  (A5Ry, green triangles).

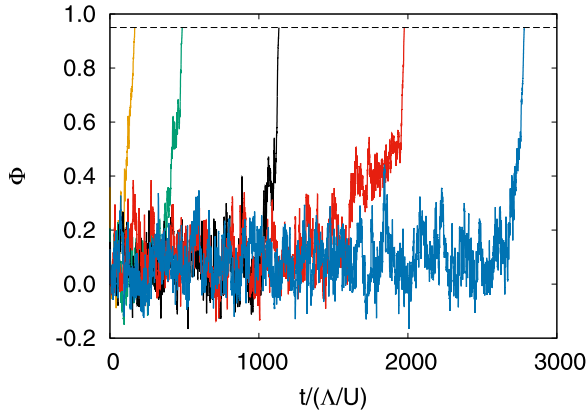


FIG. 12. Time evolution of the vortex order parameter  $\Phi$  in an ensemble of simulations A6R1 with  $\lambda = 3.5$ ,  $\alpha = -1.50$ , and  $R = 16\Lambda$ , with different initial conditions.

starting from different initial random perturbations of the null velocity field. Initially, the order parameter fluctuates around values close to 0, which is due to the disordered flow in the regime of flocking turbulence. After a long transient time  $\tau_t$  we observe a rapid increase of  $\Phi$  to a value close to 1, which signals the transition to an ordered state.

Although the simulations are performed with identical parameters, the transition time exhibits an extremely large variability on the initial condition, and this reflects the stochastic nature of the transition. The distinctive feature of the regime of flocking turbulence is the presence of many large-scale vortices [see Figs. 1(e) and 1(f)], which represent independent attempts to organize the flow in states of local flocking. In a confined domains, the competition between different vortices ends when one of them prevails over the others. Because of the chaotic dynamics of the vortices, the time at which this phenomenon occurs is unpredictable.

To quantify the variability of the transition times  $\tau_t$ , we show in Fig. 13 the probability distribution function (pdf) of  $\tau_t$ , obtained from an ensemble of 269 simulations with  $\alpha = -1.50$ ,  $\lambda = 3.5$ , and  $R = 16\Lambda$  and different initial perturbations. The transition time  $\tau_t$  is defined as the time at which  $\Phi$  exceeds the threshold value  $\Phi_{\text{thr}} = 0.95$ . The values of  $\tau_t$  span

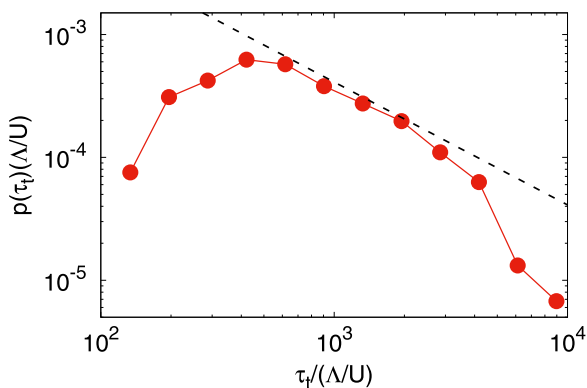


FIG. 13. Probability density function  $p(\tau_t)$  of the transition time  $\tau_t$  in the numerical simulations A6R1 with  $R = 16\Lambda$ ,  $\alpha = -1.50$ , and  $\lambda = 3.5$ . The black dashed line represents the scaling law  $\tau_t^{-1}$ .

over almost two orders of magnitude, with a maximum of the pdf at  $\tau_t \sim 40\Lambda/U$ . In the range  $500 < \tau_t/(\Lambda/U) < 4000$ , the pdf is compatible with a power-law behavior  $p(\tau_t) \sim \tau_t^{-1}$  followed by a rapid decay at larger times.

## V. CONCLUSIONS

We presented a numerical investigation of the dynamics of dense suspensions of microswimmers, described by the Toner-Tu-Swift-Hohenberg model confined in circular domains. We explored the parameter space of the model by varying the intensity of the Landau force  $\alpha$ , the self-advection parameter  $\lambda$  and the radius of the circular domain  $R$ .

We find that the model displays two different regimes, determined by the competition between the Toner-Tu terms, which promote the self-organization of the swimmers in flocks with uniform velocity, and the Swift-Hohenberg term which destabilizes the flocks and causes the formation of small vortical structures.

When the dynamics is dominated by the Swift-Hohenberg term, the velocity field consists of an homogeneous dense population of small vortices which move chaotically. In this regime of mesoscale turbulence the Landau force acts simply as a forcing term which sustains the motion of the swimmers, but they cannot develop large flocks. Conversely, when the Toner-Tu terms prevail, we observe the emergence of the flocking turbulence regime, characterized by an inhomogeneous flow with large-scale vortices surrounded by regions of uniform circular motion, alternated with regions of elongated vortical structures called streaks. Since the velocity field  $\mathbf{u}$  represents also the order parameter of the system, we can interpret the formation of these coherent structures as a spontaneous breaking of the local rotational symmetry, occurring independently in different regions of the domain.

Our study demonstrated that the self-advection term  $\lambda \mathbf{u} \cdot \nabla \mathbf{u}$  plays an important role in this transition. In particular, we find that the transition toward the flocking turbulence can be realized also keeping fixed  $\alpha$  and increasing the strength of the self-advection coefficient  $\lambda$ . These observations can be rationalized by considering the time scales of the different terms of the TTSH model. The characteristic timescale of the Landau force, of the SH term, and of the self-advection term are  $\tau_\alpha = 1/|\alpha|$ ,  $\tau_\Gamma = \Gamma_4/\Gamma_2^2$ , and  $\tau_\lambda = 1/(|\alpha|\lambda)$ , respectively. The expression of  $\tau_\lambda$  follows from the consideration that, while the typical intensity of the velocity  $U$  is determined by the Landau force, the velocity field in Eq. (1) is advected by the rescaled velocity  $\lambda U$ . In the case of pusher-like swimmers ( $\lambda > 1$ ) the self-advection time  $\tau_\lambda$  is shorter than  $\tau_\alpha$ , therefore, the transition is expected to occur when  $\tau_\Gamma \sim \tau_\lambda$ , i.e.,

$$|\alpha|\lambda \sim \frac{\Gamma_2^2}{\Gamma_4}. \quad (10)$$

Our prediction generalizes the criterion proposed in Ref. [4] for the case with constant  $\lambda$ . For  $\lambda = 3.5$  the relation (10) gives the transition value  $\alpha \simeq -1.14$ , while for fixed  $\alpha = -1$  we get  $\lambda \simeq 4$ , which are both in quantitative agreement with our numerical findings. The dependence of the transition on  $\lambda$  is an evidence of the out-of-equilibrium nature of this phenomenon. This is reminiscent of the properties of the original

Toner-Tu model, where the nonequilibrium nonlinearities are crucial in the establishment of the broken symmetry state in two-dimensions [19,22,24].

Finally, we investigated the effects of the confinement in the circular domain. Our results show that these effects become relevant when the radius of the domain is of the order of the correlation scale of the flow. In the regime of mesoscale turbulence, the correlation scale  $\xi \sim \Lambda$  is much smaller than the radius  $R$  of the domain considered in our study, therefore the flow is weakly affected by the confinement. Strong effects in this regime are expected only in the case of very small domains with  $R \sim \Lambda$ . Conversely, the correlation scale in the regime of flocking turbulence is large ( $\xi \gg \Lambda$ ); therefore, the flow is influenced by the presence of the circular boundary. We find that the friction with the boundary dissipates part of the energy and causes the production of vorticity close to the boundary. Increasing the confinement, we observe a spectral condensation of the energy in the lowest accessible mode, which causes a steepening of the energy spectrum.

Moreover, the confinement can induce a further transition toward an ordered state of circular flocking with uniform velocity, in which the swimmers are organized in a single giant vortex which spans the whole domain. The formation of this state has been previously reported in Ref. [52]. Here we show that this process has a stochastic nature which manifests in the extreme variability of the transition times. This is confirmed by the broad power-law tail of the probability distribution function of the transition times. Investigating the dependence of the statistics of the transition times on the parameters of the model requires a tremendous computational effort, which is demanded to future studies.

#### ACKNOWLEDGMENTS

We acknowledge support from the Departments of Excellence grant (MIUR) and INFN22-FieldTurb. G.B. acknowledges the Theoretical Sciences Visiting Program (TSVP) of OIST for support.

- 
- [1] M. C. Marchetti, J.-F. Joanny, S. Ramaswamy, T. B. Liverpool, J. Prost, M. Rao, and R. A. Simha, *Rev. Mod. Phys.* **85**, 1143 (2013).
  - [2] S. Ramaswamy, *Annu. Rev. Condens. Matter Phys.* **1**, 323 (2010).
  - [3] C. Dombrowski, L. Cisneros, S. Chatkaew, R. E. Goldstein, and J. O. Kessler, *Phys. Rev. Lett.* **93**, 098103 (2004).
  - [4] H. H. Wensink, J. Dunkel, S. Heidenreich, K. Drescher, R. E. Goldstein, H. Löwen, and J. M. Yeomans, *Proc. Natl. Acad. Sci. USA* **109**, 14308 (2012).
  - [5] T. Sanchez, D. T. Chen, S. J. DeCamp, M. Heymann, and Z. Dogic, *Nature (London)* **491**, 431 (2012).
  - [6] A. Doostmohammadi, J. Ignés-Mullol, J. M. Yeomans, and F. Sagués, *Nat. Commun.* **9**, 3246 (2018).
  - [7] T. B. Saw, A. Doostmohammadi, V. Nier, L. Kocgozlu, S. Thampi, Y. Toyama, P. Marcq, C. T. Lim, J. M. Yeomans, and B. Ladoux, *Nature (London)* **544**, 212 (2017).
  - [8] J. Deseigne, O. Dauchot, and H. Chaté, *Phys. Rev. Lett.* **105**, 098001 (2010).
  - [9] I. S. Aranson, D. Volfson, and L. S. Tsimring, *Phys. Rev. E* **75**, 051301 (2007).
  - [10] D. Nishiguchi and M. Sano, *Phys. Rev. E* **92**, 052309 (2015).
  - [11] A. Bricard, J.-B. Caussin, N. Desreumaux, O. Dauchot, and D. Bartolo, *Nature (London)* **503**, 95 (2013).
  - [12] R. Alert, J. Casademunt, and J.-F. Joanny, *Annu. Rev. Condens. Matter Phys.* **13**, 143 (2022).
  - [13] M. R. Shaebani, A. Wysocki, R. G. Winkler, G. Gompper, and H. Rieger, *Nat. Rev. Phys.* **2**, 181 (2020).
  - [14] M. Bär, R. Großmann, S. Heidenreich, and F. Peruani, *Annu. Rev. Condens. Matter Phys.* **11**, 441 (2020).
  - [15] L. N. Carenza, G. Gonnella, A. Lamura, G. Negro, and A. Tiribocchi, *Eur. Phys. J. E* **42**, 481 (2019).
  - [16] M. J. Bowick, N. Fakhri, M. C. Marchetti, and S. Ramaswamy, *Phys. Rev. X* **12**, 010501 (2022).
  - [17] T. Vicsek, A. Czirók, E. Ben-Jacob, I. Cohen, and O. Shochet, *Phys. Rev. Lett.* **75**, 1226 (1995).
  - [18] J. Toner and Y. Tu, *Phys. Rev. Lett.* **75**, 4326 (1995).
  - [19] J. Toner, Y. Tu, and S. Ramaswamy, *Ann. Phys.* **318**, 170 (2005).
  - [20] M. Ballerini, N. Cabibbo, R. Candelier, A. Cavagna, E. Cisbani, I. Giardina, V. Lecomte, A. Orlandi, G. Parisi, A. Procaccini *et al.*, *Proc. Natl. Acad. Sci. USA* **105**, 1232 (2008).
  - [21] H. Wioland, F. G. Woodhouse, J. Dunkel, J. O. Kessler, and R. E. Goldstein, *Phys. Rev. Lett.* **110**, 268102 (2013).
  - [22] J. Toner and Y. Tu, *Phys. Rev. E* **58**, 4828 (1998).
  - [23] H. Chaté, F. Ginelli, G. Grégoire, and F. Raynaud, *Phys. Rev. E* **77**, 046113 (2008).
  - [24] J. Toner, *Phys. Rev. E* **86**, 031918 (2012).
  - [25] A. Cavagna, L. Del Castello, I. Giardina, T. Grigera, A. Jelic, S. Melillo, T. Mora, L. Parisi, E. Silvestri, M. Viale *et al.*, *J. Stat. Phys.* **158**, 601 (2015).
  - [26] L. Chen, J. Toner, and C. F. Lee, *New J. Phys.* **17**, 042002 (2015).
  - [27] L. Chen, C. F. Lee, and J. Toner, *Nat. Commun.* **7**, 12215 (2016).
  - [28] L. Chen, C. F. Lee, and J. Toner, *New J. Phys.* **20**, 113035 (2018).
  - [29] S. Shankar, M. J. Bowick, and M. C. Marchetti, *Phys. Rev. X* **7**, 031039 (2017).
  - [30] N. Rana and P. Perlekar, *Phys. Rev. E* **102**, 032617 (2020).
  - [31] N. Rana and P. Perlekar, *Phys. Rev. E* **105**, L032603 (2022).
  - [32] J. Toner, N. Guttenberg, and Y. Tu, *Phys. Rev. E* **98**, 062604 (2018).
  - [33] L. Chen, C. F. Lee, A. Maitra, and J. Toner, *Phys. Rev. E* **106**, 044608 (2022).
  - [34] J. Dunkel, S. Heidenreich, K. Drescher, H. H. Wensink, M. Bär, and R. E. Goldstein, *Phys. Rev. Lett.* **110**, 228102 (2013).
  - [35] J. Dunkel, S. Heidenreich, M. Bär, and R. E. Goldstein, *New J. Phys.* **15**, 045016 (2013).
  - [36] J. Swift and P. C. Hohenberg, *Phys. Rev. A* **15**, 319 (1977).
  - [37] M. James, W. J. T. Bos, and M. Wilczek, *Phys. Rev. Fluids* **3**, 061101(R) (2018).
  - [38] H. Reinken, S. H. L. Klapp, and M. Wilczek, *Phys. Rev. Fluids* **7**, 084501 (2022).

- [39] V. Bratanov, F. Jenko, and E. Frey, *Proc. Natl. Acad. Sci. USA* **112**, 15048 (2015).
- [40] M. James and M. Wilczek, *Eur. Phys. J. E* **41**, 21 (2018).
- [41] S. C. P. and A. Joy, *Phys. Rev. Fluids* **5**, 024302 (2020).
- [42] Y. Xia, X. Qiu, J. Lou, and Y. Qian, *Physica A* **555**, 124402 (2020).
- [43] M. James, D. A. Suchla, J. Dunkel, and M. Wilczek, *Nat. Commun.* **12**, 5630 (2021).
- [44] F. Zanger, H. Löwen, and J. Saal, in *Mathematics for Nonlinear Phenomena—Analysis and Computation*, edited by Y. Maekawa and S. Jimbo (Springer International Publishing, Cham, 2017), pp. 285–303.
- [45] S. Mukherjee, R. K. Singh, M. James, and S. S. Ray, *Phys. Rev. Lett.* **127**, 118001 (2021).
- [46] R. K. Singh, S. Mukherjee, and S. S. Ray, *Phys. Rev. Fluids* **7**, 033101 (2022).
- [47] S. Mukherjee, R. K. Singh, M. James, and S. S. Ray, *Nat. Phys.* (2023).
- [48] N. A. Araújo, L. M. Janssen, T. Barois, G. Boffetta, I. Cohen, A. Corbetta, O. Dauchot, M. Dijkstra, W. M. Durham, A. Dussutour *et al.*, *Soft Matter* **19**, 1695 (2023).
- [49] H. Wioland, E. Lushi, and R. E. Goldstein, *New J. Phys.* **18**, 075002 (2016).
- [50] K. Beppu, Z. Izri, J. Gohya, K. Eto, M. Ichikawa, and Y. T. Maeda, *Soft Matter* **13**, 5038 (2017).
- [51] D. Nishiguchi, I. S. Aranson, A. Snezhko, and A. Sokolov, *Nat. Commun.* **9**, 4486 (2018).
- [52] L. Puggioni, G. Boffetta, and S. Musacchio, *Phys. Rev. E* **106**, 055103 (2022).
- [53] S. Heidenreich, J. Dunkel, S. H. L. Klapp, and M. Bär, *Phys. Rev. E* **94**, 020601(R) (2016).
- [54] H. Reinken, S. H. L. Klapp, M. Bär, and S. Heidenreich, *Phys. Rev. E* **97**, 022613 (2018).
- [55] E. Arquis, J. Caltagirone *et al.*, *CR Acad. Sci. Paris II* **299**, 1 (1984).
- [56] K. Schneider and M. Farge, *Phys. Rev. Lett.* **95**, 244502 (2005).
- [57] K. Schneider, M. Paget-Goy, A. Verga, and M. Farge, *Comp. Appl. Math.* **33**, 481 (2014).
- [58] A. Okubo, in *Deep Sea Research and Oceanographic Abstracts* (Elsevier, Amsterdam, 1970), Vol. 17, pp. 445–454.
- [59] J. Weiss, *Physica D* **48**, 273 (1991).
- [60] K. V. Kiran, A. Gupta, A. K. Verma, and R. Pandit, *Phys. Rev. Fluids* **8**, 023102 (2023).
- [61] See Supplemental Material at <http://link.aps.org/supplemental/10.1103/PhysRevE.107.055107> for two short movies of the formation of the flocking turbulence and of the giant vortex.
- [62] A. Cavagna, I. Giardina, and T. S. Grigera, *Phys. Rep.* **728**, 1 (2018).
- [63] E. Lushi, H. Wioland, and R. E. Goldstein, *Proc. Natl. Acad. Sci. USA* **111**, 9733 (2014).